Chapter 5

Metal Oxide-Polymer Hybrid Bilayer Devices

After the successful demonstration of aluminum oxide based RRAM devices, it is imparative to further enhance the RRAM perfomance on parameters such as the switching voltage, memory window, retention time, and endurance. To address these issues, a concept of "Hybrid RRAM" is introduced in this part the thesis dissertation where a bilayer structure of poly(4-vinylphenol) and hafnium oxide has been used as the switching layer [Varun *et al.*, 2018]. The fabricated devices were explored for their switching performance and reliability in the chapter.

5.1 INTRODUCTION TO HYBRID RRAM

Over the past ten years, profound research interest in the field of conductive bridge resistive random access memories (CBRAMs) has been developed due to its simple structure, easy fabrication, lower power consumption, scaling, integration capabilities with CMOS technology, and multibit storage ability [Daniele, 2016]. Resistive switching has been investigated in various inorganic and organic dielectrics such as like HfO_2 [Saadi *et al.*, 2016], Al_2O_3 [Varun *et al.*, 2017], Ta_2O_5 [Gao *et al.*, 2015], TiO_2 [Park *et al.*, 2010], ZnO [Peng *et al.*, 2010], poly(methyl-methacrylate) [Mangalam *et al.*, 2016], Cu:tetracyanoquinodimethane [Kever *et al.*, 2007], polyvinyl alcohol [Lin *et al.*, 2014b], poly(4-vinylphenol) (PVP) [Sun *et al.*, 2015], graphene oxide [Hazra *et al.*, 2016], and poly(vinylpyrrolidone) [Ali *et al.*, 2015]. Switching mechanisms in these CBRAM devices have been found mainly due to electro-migration of electrode ions through the dielectrics or the oxygen vacancies in the oxide films [Michael and Hugh, 2016; Park and Lee, 2016]. Organic dielectrics based CBRAM devices are known for their excellent switching window whereas the metal oxide based CBRAMs are popular for their reliability, longer retention time and low voltage operation [Cho *et al.*, 2011; Daniele, 2016; Vyas *et al.*, 2016]. The qualities of each type of dielectric are expected to evolve collectively in their hybrid stacks. Though there are various reports available on metal oxide based bilayer CBRAMs to obtain improved performance, only a few reports are available on organic dielectrics and their stacks [Akbari *et al.*, 2017; Yefan *et al.*, 2014; Zhang *et al.*, 2015]. Poly(4-vinylphenol) (PVP)/HfO_x stack has resulted in devices with low operating voltage and uniform performance when used as gate dielectric in organic field effect transistors (OFETs) and OFET based sensors, however the capabilities of this stack as an insulating medium in CBRAMs to obtain lower operating voltages and uniform performance are yet to be examined [Bharti *et al.*, 2017].

In this chapter, we report bipolar resistive switching in PVP/HfO_x based low voltage and highly reliable hybrid CBRAM devices. The weibull distribution of set (V_{set}) and reset (V_{reset}) voltages indicates a reliable device performance. In addition, a low device-to-device variability was confirmed from similar switching properties of 10 random devices of the sample. The morphological study of PVP revealed presence of pinholes which assist the electro-migration of top electrode (TE) ions through PVP layer and HfO_x thin film, switching the device to low

resistance state (LRS). Depth of these pinholes gets smaller with increasing the PVP concentration which results in lower switching voltages. The electrochemical and joule-heating assisted rupture of CF drives the device back to high resistance state (HRS). The pinholes formed at PVP surface has been exploited to obtain a low voltage and reliable switching operation as it restrains the formation of multiple conductive filaments in the switching layer and hence a low voltage reset process.

5.2 DEVICE FABRICATION

CBRAM devices with PVP/HfO_x bi-layer were fabricated on cleaned Indium Tin Oxide (ITO) coated glass substrates. The bottom ITO layer is acting as bottom electrode (BE) over which an ultra-thin HfO_x layer of ~5 nm thickness was deposited at 100 °C chamber temperature using atomic layer deposition system with tetrakis(dimethylamido)hafnium (TDMAH) and H_2O as precursors. The solution for second dielectric layer of PVP was prepared by ultrasonication of 2.5 wt%, 3.5 wt.%, and 4.5 wt.% PVP (M_w ~ 25,000) in 2-propanol for 30 minutes for preparing three samples with different PVP concentrations. The solution was spin coated at 7000 rpm for 1 minute to obtain ~130 nm thick PVP layer. The samples were kept in vacuum for 12 hours for complete solvent evaporation. Finally, 150 nm thick Ag top TE were thermally evaporated under a high vacuum of 10^{-6} torr and patterned through circular metal shadow mask.. The surface morphology of PVP film was analyzed by using XE70 atomic force microscope (AFM) from Park systems in noncontact mode. The cross-sectional field emission scanning electron microscopy (X-FESEM) was performed to carry out the interfacial study of the PVP/HfO_x/ITO layers.

5.3 RESULTS & DISCUSSIONS

5.3.1 Film Characterization

The schematic of fabricated device is shown in Figure 5.1(a). X-FESEM of PVP (2.5 wt.%)/HfO_x/ITO stack shows smooth interface of three layers in Figure 5.1(b). The AFM scan of PVP film confirms a smooth surface in 2.5 wt%, 3.5 wt.%, and 4.5 wt.% PVP samples displaying displaying the root mean square (RMS) roughness of 3.05 nm, 1.33 nm, and 0.42 nm respectively. Surface morphology of PVP film exhibits the presence of pin holes with depth of ~42 nm and ~13.5 nm at x and y locations in 2.5 wt.% sample, 4.2 nm in 3.5 wt.% sample, 1.6 nm in 4.5 wt.% sample as shown in Figure 5.1(f-h) respectively [Vyas *et al.*, 2016]. Hence we can say that the depth of pinholes is reducing and surface smoothness is improving with increased PVP concentration. These pinholes are filled with Ag after TE deposition.

5.3.2 Switching Performance & Reliability

The electrical characterization of devices was carried out by keeping BE at the ground potential and biasing was applied at the TE. Compliance current of 10 mA was applied to protect the devices from permanent breakdown. The pristine devices were in inherent HRS and an initial forming process was performed to activate the devices. Figure 5.2(a) shows the forming process in the devices, where the switching happens in the device for the first time at V_f = 1.94 V in 2.5 wt.% devices and V_f = 2.58 V in 3.5 wt.% devices. As displayed in Figure 5.2(b), devices with 4.5 wt.% PVP didn't exhibit resistive switching characteristics even at higher sweep voltages of 12 V. In subsequent switching event, the 2.5 wt.% device remain in HRS at lower values of applied bias and switches to LRS with a sharp rise in current at V_{bias} = V_{set} = 1.03 V. Device continues to show conductive behavior until the applied bias is swept to V_{reset} = -0.68 V, which switches the device back to HRS. On the other hand, the 3.5 wt.% RRAM device demonstrated the set and reset process at V_{set} = 1.48 V and V_{reset} = -0.82 V as shown in Figure 5.2(c). The 2.5 wt.% devices were considered for further exploration of switching properties due to its low voltage switching operation. The results discussed from here onwards will be of Ag/PVP (2.5 wt.% PVP)/ HfO_x/ITO devices unless stated. Figure 5.2(c) shows the current- voltage (*I-V*) curves of device

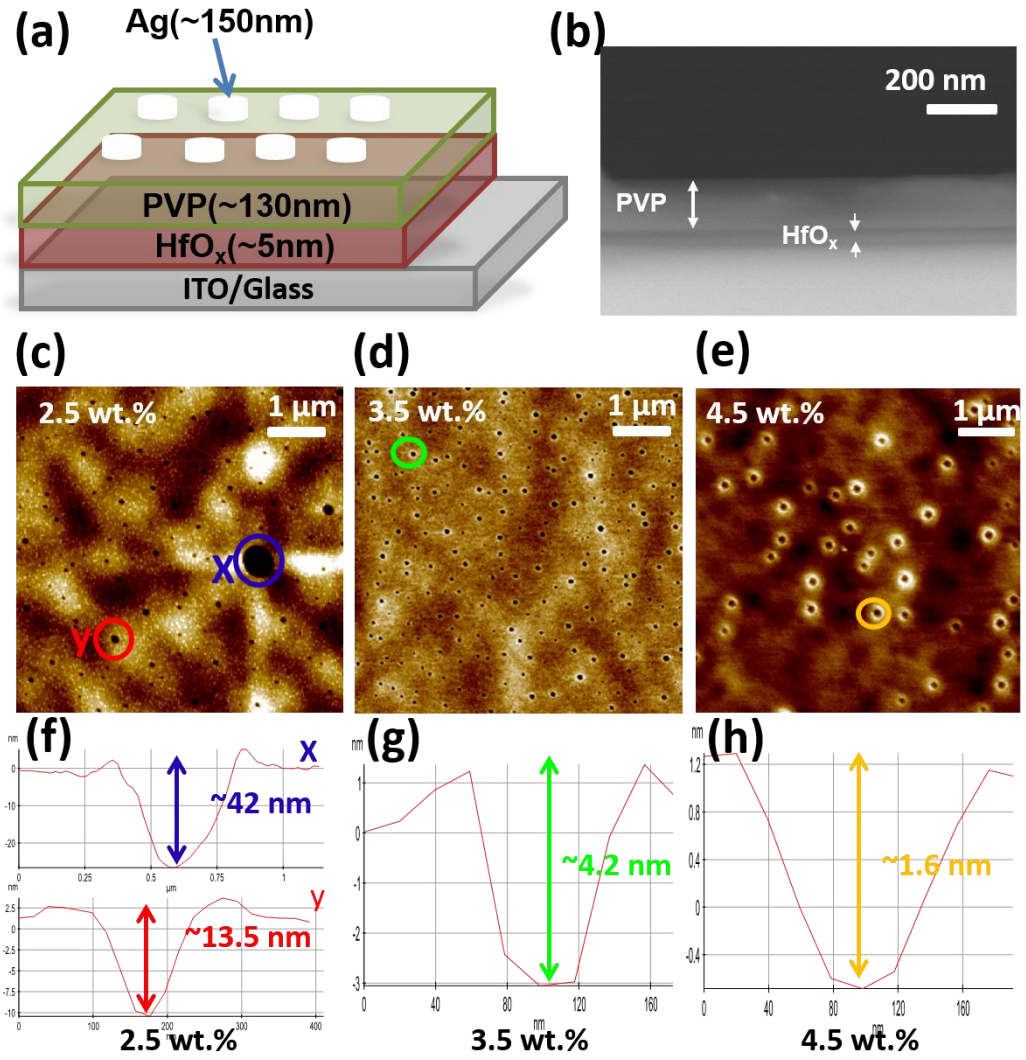

Figure 5.1: (a) Device schematic with thicknesses of respective layers, **(b)** X-FESEM image of PVP/HfO_x/ITO, **(c-e)** AFM image of 2.5 wt.%, 3.5 wt.%, and 4.5 wt.% PVP film with scan area of 5 × 5 μm^2 showing RMS roughness of 3.05 nm, 1.33 nm, 0.42 nm respectively, and **(f-h)** shows the corresponding line profiles of encircled region indicating pinhole formation with depth of ~42 nm and ~13.5 nm at x and y locations respectively in 2.5 wt.%, ~4.2 nm in 3.5 wt.%, and ~1.6 nm in 4.5 wt.% respectively.

clearly demonstrating the bipolar resistive switching with I_{on}/I_{off} of 80 at −0.2 V. Figure 5.2(d) shows repeatability of 300 DC cycles at nearly uniform switching voltages and the variation of V_{set} and V_{reset} with number of cyclic operation, which largely maintain consistency with number of cycles has been demonstrated in Figure 5.2(e). The device-to-device variation of the switching and forming voltages of 10 devices chosen randomly for testing has been shown in Figure 5.2(f). Data retention capability of device was tested by applying a constant read voltage V_{read} = 0.2 V in LRS and V_{read} = -0.2 V in HRS. Figure 5.3(a) shows 7200 s of retention time in the respective states, without any degradation in current levels. The endurance test of device was carried out by applying 2000 AC pulses with each pulse having pulse width of 100 ms with alternate set andreset pulse values of 1.9 V and -1.6 V respectively as shown in Figure 5.3(b). The after-effect of consecutive set and reset process during endurance test is shown in inset which displays an unclear set. The reliability analysis of device is performed using weibull's distribution to display the variation in sw itching voltages of the device over the number of operating/switching cycles as shown in Figure 5.3(c). The shape factor βv and maximum spread of 22 and 0.24 V for V_{set} and 14 and 0.34 V for V_{reset} were obtained respectively, confirming a reliable device performance [Lawless, 2002].

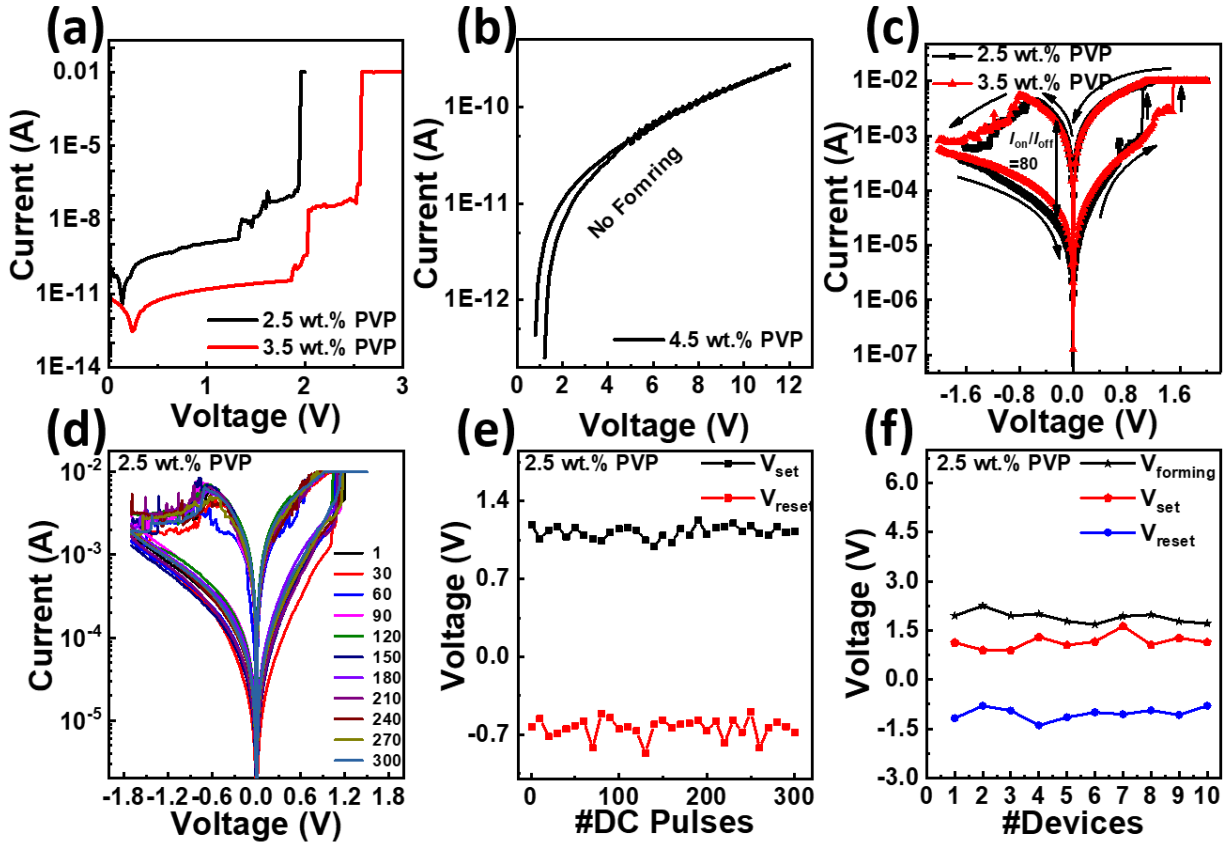

Figure 5.2: (a) The forming process at V_f = 1.94 V in 2.5 wt.% device and V_f = 2.58 V in 3.5 wt.% device. **(b)** Also, the *I-V* curve of 4.5 wt.% is not demonstrating resistive switching till 12 V. **(c)** *I-V* curve showing switching behavior of CBRAM devices with 2.5 and 3.5 wt% PVP.. **(d)** 300 cycles of repeatable switching operation, **(e)** variation in V_{set} and V_{reset}, and **(f)** switching parameters of 10 devices illustrating the device-to-device variability.

5.3.3 Conduction & Switching Mechanism

To understand the conduction mechanism, *I-V* curve in Figure 5.2(a) was plotted on double log scale, as shown in Figure 5.3(d). HRS region can be divided into two parts, an ohmic conduction region where $I \propto V$ at low biasing and $I \propto V^{2.3}$ at higher bias voltages signifying trap filled space charge limited conduction (TF-SCLC). Expression for TF-SCLC can be given as:

$$J_{TF} = 9\varepsilon_m \mu \theta V^2 / 8d^3 \qquad (5.1)$$

where ε_m represents dielectric constant of material, μ is the mobility of charge carriers, θ is ratio of free to total carrier density, V the applied bias, and d the separation between two electrodes [Shang *et al.*, 2006; Wright, 1961]. Moreover, once the device is set, the complete LRS region will follow the ohmic conduction demonstrating the metallic behavior of the CF. After the application of bias across the electrodes, there will be generation of oxygen vacancies under the effect of extremely high electric field which will act as trap sites for the charge injected from BE [Park and Lee, 2016; Sharath *et al.*, 2014]. Under the applied bias, the oxygen vacancy generation in the HfO_x thin film can be explained using Kroger-Vink notation [Kröger and Vink, 1958]:

$$O_o^x \rightleftharpoons V_o^{2+} + 2e^- + \frac{1}{2}O_2 \qquad (5.2)$$

where O_o^x is oxygen ion on an oxygen site and V_o^{2+} is the oxygen vacancy with 2+ charge.

The switching mechanism in Ag/PVP/HfO_x/ITO CBRAM devices can be demonstrated using a schematic diagram shown in Figure 4(a), where the CF formation is assisted by electro-migration of Ag^+ ions in PVP layer and HfO_x thin film [Saadi *et al.*, 2016]. When positive bias is applied on the TE, oxidation of Ag atoms ($Ag - e^- \rightarrow Ag^+$) occurs resulting in generation of Ag^+ ions, which are electro-migrated through the PVP and HfO_x layers towards the ITO BE as shown in Figure 4(b)(i) [Yang *et al.*, 2009; Yiming Sun, 2017]. The Ag^+ ions after reaching the ITO BE will

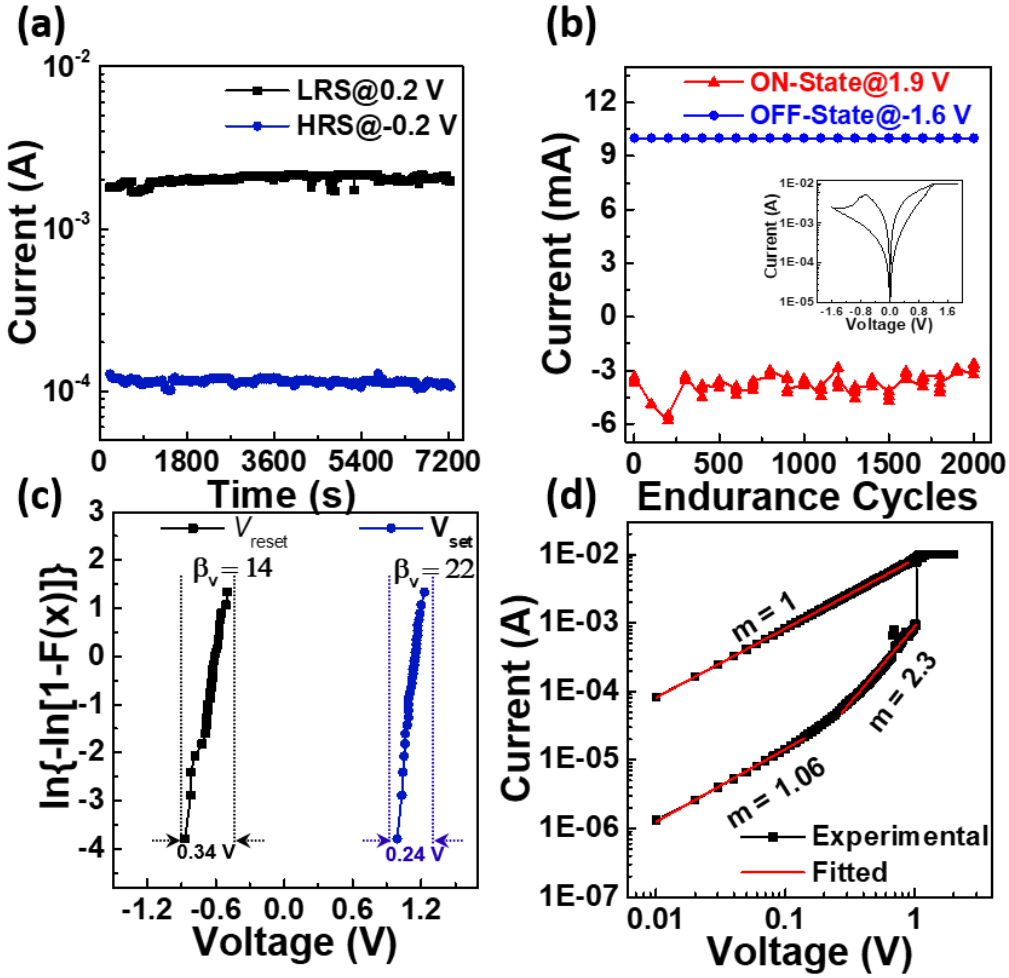

Figure 5.3. (a) Plot of Retention time measurement by applying read voltages of -0.2 V and 0.2 V in HRS and LRS respectively, showing retention time of 72000 sec without degradation in current levels, **(b)** AC endurance of device showing the capability to withstand continuous switching for more than 2000 cycles. **(c)** Weibull's distribution for reliability test of the CBRAM device, and **(d)** double log I-V curve showing ohmic and TF-SCLS conduction mechanisms.

be reduced to Ag atoms ($Ag^+ + e^- \rightarrow Ag$) while interacting with the electrons injected from the BE. Figure 4(b)(ii) shows that once all the Ag^+ ions get reduced to Ag atoms, the CF is formed and device is switched to LRS. The probability of electro-migration of Ag^+ ions under high electric field is more at the locations of deep pinholes (with depth of up to 42 nm in the ~130 nm thick PVP layer) present on the PVP surface, which are filled with Ag during the TE deposition process as displayed through Figure 4(b)(i) [Yiming Sun, 2017]. During the reset process, with the polarity of bias reversed, the electrochemical and joule-heating assisted rupture of CF takes place across the position where current density and electric field concentration is maximum i.e. the tip of pinholes, restoring the device back in its initial HRS, as shown in Figure 4(c) [Yang *et al.*, 2009; Yefan *et al.*, 2014; Yiming Sun, 2017]. A 10 mA of current flowing through CF of few nanometers diameter, resulting in current density as high as 10^9 A/cm^2, is enough to cause the localized joule heating and hence rupture of CF. As observed in previous reports, the Ag CF in a conventional CBRAM can take an irregular shape with many branches, which in turns make it difficult to completely dissolve the CF during the reset process [Yang *et al.*, 2009]. This results in degraded reliability of CBRAM devices. In the reported Ag/PVP/HfO_x/ITO CBRAM devices, the pinhole tip guides the growth of CF and can control the number of CFs formed, and thus, regulate the dissolution of CF during reset process [Yiming Sun, 2017]. This well regulated reset process has resulted in lower switching voltages and reliable operation.

Performance of organic and inorganic CBRAMs in pure and hybrid configurations is compared in Table I. Though PVP/HfO_x hybrid devices in this study exhibit moderate switching, simultaneous achievement of lower switching voltages,comparable retention time, and higher

endurance than most of the other configurations are some of the distinguishable features of these devices. In addition, this study also reports sample yield (> 75%, 10 out of 13 devices on a sample), a significant performance metric, but yet rarely remarked.

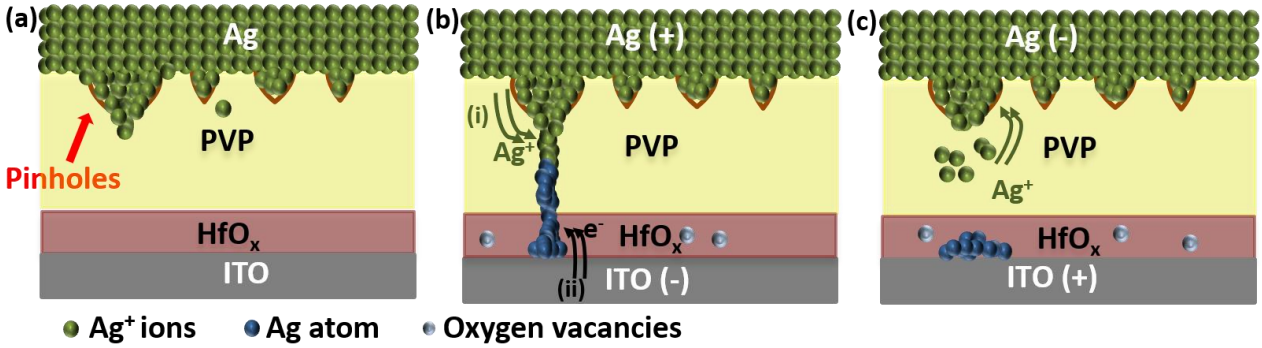

Figure 5.4. (a) Schematic illustrating the device structure with pinholes in PVP layer filled with Ag. **(b)(i)** Oxidation of Ag to Ag^+ ions and diffusion of Ag^+ ions into PVP layer through the pinholes, **(ii)** reduction of Ag^+ ions to Ag atoms and formation of CF by Ag atoms. **(c)** On reversal of bias polarity, electrochemical joule-heating assisted rupture in CF at the pinholes tip due to high current density and electric field concentration.

Table 5.1. Comparison of electrical characteristics of samples in terms of following parameters.

Dielectric layer	Memory Window	V_{set} (V)	V_{reset} (V)	Endurance (cycles)	Retention time (s)	Sample yield (Devices)	Ref.
HfO_x	10^2	0.5	-0.6	50	2000	N/A	[Labalette *et al.*, 2017]
PMMA	10^3	1.4	-2.1	400 s	300	N/A	[Mangalam *et al.*, 2016]
PMMA+ HfO_x	10	0.8	-0.75	10^3	10^4	N/A	[Jae-Won and Won-Ju, 2017]
PVP +DDQ	10^6	3	1.3	20	10^3	N/A	[Vyas *et al.*, 2016]
PVP +PBD	10^4	-1.4	3.55	300	3×10^4	N/A	[Sun *et al.*, 2015]
MoS_2/ PVA	10^2	3	-3	10^3	$>10^5$	N/A	[Rehman *et al.*, 2016]
HfO_x/parylene-c	10^3	-2	0.60	N/A	10^4	N/A	[Yefan *et al.*, 2014]
PVP/ HfO_x	80	1.03	-0.68	2000	7200	>75%	This work

Good- Green *Bad-Red* *Moderate-Blue*

5.4 CONCLUSION

The Ag/PVP/HfO_x/ITO hybrid CBRAM with 2.5 wt.%, 3.5 wt.% and 4.5 wt.% PVP concentrations has been studied for their resistive switching behavior and reliability. As observed from the I-V characteristics of devices, forming, set, and reset voltages have reduced with increasing PVP concentration. This can be attributed to the decreased pinhole depth with increased PVP concentration and which in turns develops an adverse environment for filament formation. Low voltage and highly reliable bipolar resistive switching behavior with decent repeatability was observed in these devices. High yield and very small device-to-device deviation with nearly same switching parameters of 10 tested devices were obtained. The low voltage and stable switching operation was attributed to the pinholes assisted electro-migration of Ag^+ ions

through the PVP layer and HfO_x thin film, and upon reversing the bias voltage, the electrochemical and joule-heating causes the CF to rupture across the pinholes tips due to high current density and electric field concentration at the junction. The pinholes formation at PVP surface also benefited the growth of a dedicated CF instead of multiple filaments that is difficult to dissolve and causes inferior device performance.